ADVANCED FUNCTIONAL MATERIALS
www.afm-journal.de

Endothelial Cells Angiogenesis in Sulfated Glycosaminoglycan (GAG) Hydrogels Enhanced by Bioactive Glass-Released Ions

Marco Piazzoni, Ilaria Borghi, Francesca Cadamuro, Sophia Dalfino, Riccardo Campanile, Sofia Nizzolo, Valeria Cassina, Francesca Tallia, Julian R. Jones, Francesco Mantegazza, Sabrina Bertini, Lorenzo Moroni, Francesco Nicotra, and Laura Russo**

The successful clinical translation of large-scale tissue-engineered constructs is significantly hindered by the lack of functional vascularization, which is crucial for delivering oxygen and nutrients to cells. Current in vitro angiogenesis models often rely on murine tumor-derived extracellular matrix (ECM) materials, which suffer from non-defined composition and batch-to-batch variability, and on the delivery of growth factors at non-physiological concentrations. Hydrogels offer a superior alternative for the rational design of biomimetic ECM environments, because of their versatility in tuning biochemical and mechanical properties. This study presents a novel growth factor-free hydrogel composed of gelatin, chondroitin sulfate, and laminin, designed to promote endothelial cell (EC) angiogenesis in vitro. The hydrogel's mechanical properties are precisely controlled by varying its crosslinking degree, attesting that a softer substrate (Young's modulus ≈80 Pa) significantly boosts ECs tube formation. Furthermore, the angiogenic process is enhanced by several hours with ions released by bioactive glass 58S (BG58S), specifically calcium and silicon. Finally, the expression of angiogenesis-related genes and the production of matrix remodeling enzymes is augmented in the presence of BG58S-conditioned medium. It is believed that this bioinstructive sulfate GAG based hydrogel represents a promising solution for vascularizing 3D cellular constructs, marking a significant step toward the clinical application of tissue engineering products.

1. Introduction

Vascularization of biological substitutes represents a real issue for the clinical translation of tissue engineering products. [1,2] As a matter of fact, the development of 3D cellular constructs with a clinically relevant size (>1 cm^3)[3–5] is currently hampered by the inability to establish a functional vasculature able to sustain oxygen and nutrients delivery to growing tissues.[6–8]

The human body can generate new blood vessels from preexisting ones through the process of angiogenesis.[9] The best effort to recapitulate this morphogenic process in vitro was achieved with the employment of biomaterials able to mimic the extracellular matrix (ECM),[10–12] and in particular, the basement membrane (BM), so to instruct endothelial cells (EC) to activate the angiogenic molecular pathways.[13] In vitro tests are usually done with commercial ECM-based materials derived from murine sarcoma tumor extracts (i.e., Matrigel). Nonetheless, the unknown exact

M. Piazzoni, I. Borghi, F. Cadamuro, R. Campanile, V. Cassina, F. Mantegazza, F. Nicotra, L. Russo
School of Medicine and Surgery
Università degli Studi Milano-Bicocca
Vedano al Lambro (MB), Italy
E-mail: marco.piazzoni@unimib.it; laura.russo@unimib.it

S. Dalfino, L. Moroni
Complex Tissue Regeneration
MERLN Institute for Technology-Inspired Regenerative Medicine
Maastricht University
Maastricht 6229 ER, the Netherlands

The ORCID identification number(s) for the author(s) of this article can be found under https://doi.org/10.1002/adfm.202519933

DOI: 10.1002/adfm.202519933

S. Dalfino
Department of Biomedical Sciences for Health
Università degli Studi di Milano
Milano, Italy

S. Dalfino
Department of Biomedical
Surgical and Dental Sciences
Università degli Studi di Milano
Milano, Italy

S. Nizzolo, S. Bertini
Istituto di Ricerche Chimiche e Biochimiche "G. Ronzoni"
Milano, Italy

F. Tallia, J. R. Jones
Department of Materials
Imperial College London
South Kensington Campus, London SW7 2AZ, UK

L. Russo
Fondazione IRCCS San Gerardo dei Tintori
Monza, Italy

composition, batch-to-batch variability, and the impossibility of adjusting material types and quantities make them an obsolete option in tissue engineering.[14,15] Within this context, hydrogels represent the most valuable candidates to engineer ECM mimics with a bottom-up approach, due to the possibility of finely tuning their biochemical composition and mechanical properties.[16,17]

The BM is primarily made of collagen IV, laminins (LM), nidogen/entactin, and heparan sulfate proteoglycans (HSPG), each of which is involved in specific functions during angiogenesis.[18] For such reason, efforts have been made to design hydrogel systems incorporating these macromolecules either as complete structures or via the integration of specific functional domains only. The most used strategies to generate synthetic BM consist of covalently linking to a hydrogel peptide sequences of LM (e.g., SIKVAV and YIGSR)[19] or of collagen (e.g., RGD)[20] to ensure ECs attachment to the substrate. However, to ensure functional BM, sulfated glycosaminoglycans (GAG) proved also to be needed. Thanks to their negatively charged sulfate groups, GAGs have the ability to selectively interact with positively charged molecules, like the vascular endothelial growth factor (VEGF), the fibroblast growth factor (FGF), and other chemokines, favoring their stabilization and angiogenetic activity.[21] Both heparan sulfate (HS)[22,23] and chondroitin sulfate (CS)[24] -based hydrogels were indeed reported as extremely effective biomaterials, considering that they have similar charge density and sulfation patterns.[25]

Furthermore, since material stiffness was proven to have a great impact on ECs ability to organize in tubule-like structures, hydrogels with tunable mechanical properties were developed.[26]

Despite these promising results, the majority of hydrogels required VEGF administration at concentrations (μg mL^{-1} range) far superior to what is normally found in vivo (pg mL^{-1} range) in order to effectively induce tube formation,[27] thus limiting their therapeutic use in advanced engineering methods.[28] A valid alternative to growth factors administration are inorganic ions. Within this context, bioactive glasses (BG) not only can stimulate new bone growth, but can also act as angiogenic promoter through their dissolution products.[29–31] Upon contact with physiological solutions (e.g., simulated body fluid (SBF), culture media) BG releases ions (e.g., Si, Ca) that can induce lots of different biological activities.[32,33] Several works have indeed demonstrated the ability of BG to increase ECs proliferation and migration ability, key initial steps of angiogenesis.[24,34]

Here we report a hydrogel made of gelatin (GEL), CS, and LM to promote ECs angiogenesis in vitro without the addition of external growth factors. Moreover, the morphogenic process proved to be kinetically enhanced by medium conditioned with bioactive glass 58S (BG58S). CS and GEL were functionalized with a methyl-furan moiety to undergo a Diels Alder cycloaddition with 4arm-PEG10k-Maleimide, enabling precise control of hydrogel crosslinking density. This fine-tuning allowed modulation of the material Young's modulus (E) at the micro-nanoscale as demonstrated through Atomic Force Microscopy (AFM) measurements, greatly enhancing ECs migration ability and mesh organization on softer substrates (E ≈80 Pa). Medium conditioned with BG58S improved ECs viability and accelerated tube formation by several hours through the release of calcium and silicon. Moreover, upregulation of angiogenesis-related genes and increased secretion of matrix remodeling enzymes suggested that Ca and Si participate at multiple levels to regulate the molecular pathway, that leads to the establishment of cell-cell junctions and ECM degradation. We believe that this growth factor-free GAG-based hydrogel might be a suitable solution to vascularize 3D cellular constructs in vitro, making a step forward the clinical translation of tissue engineering products.

2. Results and Discussion

2.1. Hydrogel Rational Design and Characterization

ECs are in contact with a thin but highly specialized ECM layer: the basal membrane. Hydrogels were designed to bear fundamental biomolecules normally found in this structure in order to recapitulate the complex molecular machinery that leads to angiogenesis in vivo. In particular, gelatin (being the hydrolyzed form of collagen) was introduced to support cell adhesion through the RGD domains[18]; whereas CS, being a sulfated GAG, was used for its capacity to interact with pro-angiogenic growth factors bearing positive charges (e.g., VEGF, FGF), leading to their stabilization and localization in the hydrogel.[18,21]

In particular, in this study, a CS with an average molecular weight (Mw) of 30 kDa and a polydispersity index of 1.3 was used (Table S1, Supporting Information). The sulfate (SO_{3-}) to carboxyl (COO^-) group ratio was found to be ≈1.07 and the 4-sulfate to 6-sulfate (4S/6S) ratio was equal to 2.55, as determined respectively by conductometric titration (Supporting Information) and HSQC experiments (Figure S3, Supporting Information). Both the sulfate-to-carboxyl ratio and the 4S/6S sulfation pattern were thus coherent with the CS molecular structure characteristics that are known to support ECs angiogenesis.[35,36]

GEL and CS were first functionalized with 5-methylfuran (5MF) groups. In detail, the amine groups on lysine residues of gelatin were functionalized via reductive amination with 5-methylfurfural. In contrast, CS was functionalized with 5-methylfurfurylamine through a carbodiimide-mediated coupling reaction involving its carboxylic acid groups. The DoF, determined by ^{1}H NMR spectroscopy, resulted to be around 100 % of the lysine moieties for GEL-5MF and 13 % for CS-5MF (Figures S1,S2, Supporting information).

Functionalized polymers were then crosslinked together with a 4arm-PEG10k-Maleimide through Diels-Alder (DA) reaction (**Figure 1A**). This cycloaddition is a click chemistry reaction, which proceeds with high chemoselectivity between the diene groups on the polymers and the dienophile on the linker, yielding covalent crosslinks.

Varying hydrogel GEL-5MF:CS-5MF % w/w ratios and crosslinking degree (γ) proved to efficiently change the material storage modulus (Figure 1B) of nearly two orders of magnitude (from 58 to 1450 Pa), attesting extreme mechanical tunability.

Hydrogels with GEL-5MF:CS-5MF % w/w ratios of 2:1 and a crosslinking degree of 100 (H-1) and 50 (H-0.5) were proven to be superior in inducing EC morphogenesis compared to

L. Russo
CURAM Research Ireland Centre for Medical Devices
University of Galway
Ireland

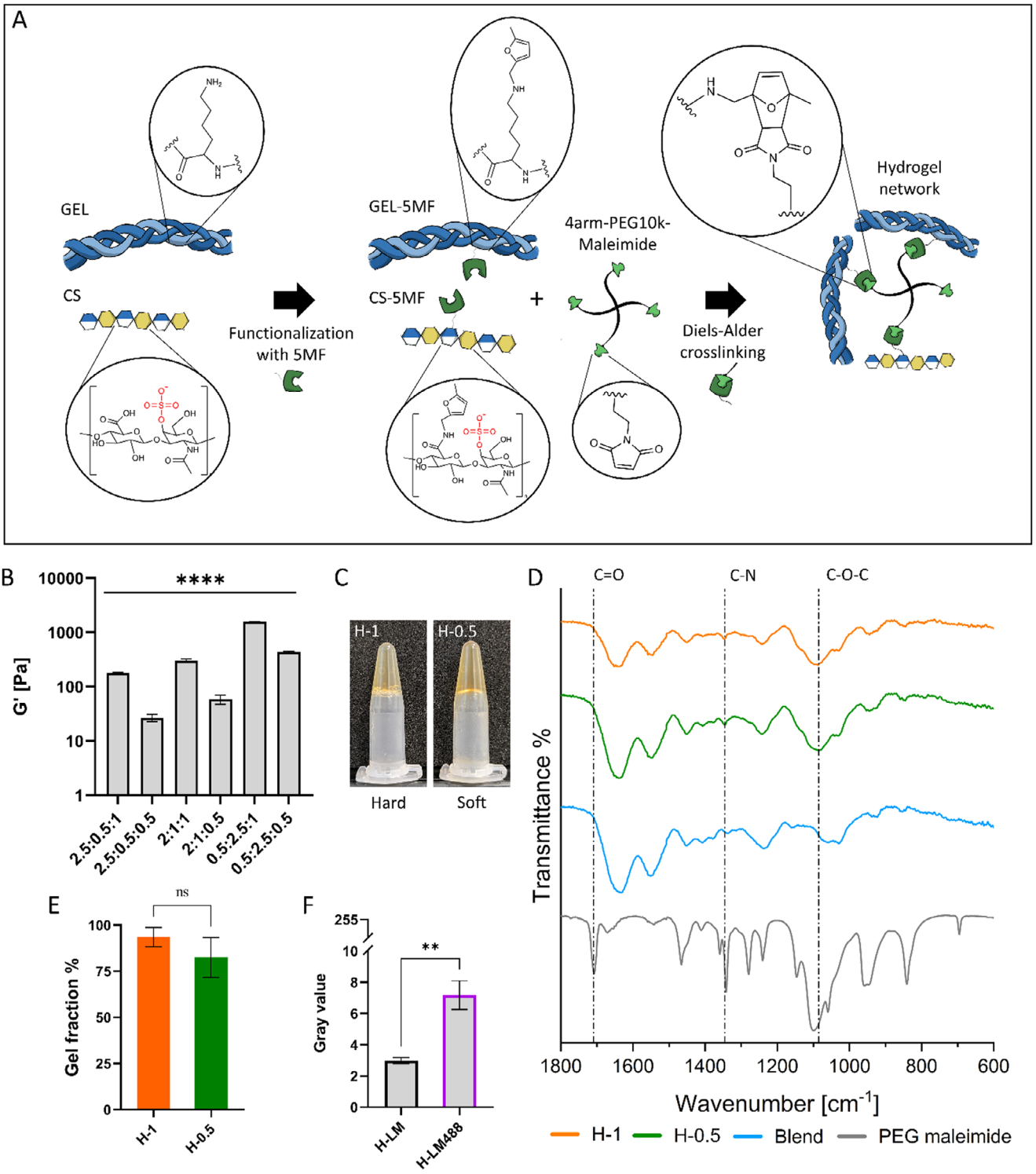

Figure 1. A) Illustration of the materials functionalization with 5MF and crosslinking with 4arm-PEG10k-Maleimide. B) Storage modulus of hydrogels changing GEL-5MF:CS-5MF % w/w ratios (i.e., 2.5:0.5, 2:1, 0.5:2.5). C) A representative picture of crosslinked hydrogel formulations H-1 (left) and H-0.5 (right). D) FT-IR spectra of crosslinked H-1 and H-0.5 hydrogel formulations, 4arm-PEG10k-Maleimide (PEG maleimide) and of a mixed GEL-5MF and CS-5MF (Blend). Dashed lines indicate: C═O stretching (1709 cm^{-1}), C—N stretching (1345 cm^{-1}), C—O—C bending (1080 cm^{-1}). E) Gel fraction % of hydrogel formulations. F) Grayscale values of images taken at the fluorescence microscope for a hydrogel coated with LM (H-LM) and a hydrogel coated with LM-DyLight 488 (H-LM488). Data (n = 3) are presented as mean ± SD. Non-significant (ns), $p > 0.05$, $^{**}p \leq 0.01$, $^{****}p \leq 0.0001$.

other formulations (Figure S4, Supporting Information), therefore further experiments were conducted only on these hydrogels (Figure 1C).

The presence of the DA adduct was confirmed by FT-IR spectroscopy (Figure 1D). The characteristic bands of symmetric C—O—C stretching (1080 cm^{-1}) and C—N stretching (1345 cm^{-1}) were indeed present in crosslinked hydrogel formulations (H-1 and H-0.5) but not in the mixed GEL-5MF and CS-5MF (Blend).[37] Notably, the C═O stretching (1709 cm^{-1}) assigned to the maleimide groups also disappeared after hydrogel crosslinking, supporting the involvement of the maleimide moiety in the cycloaddition reaction.[38] Gel fraction experiments also attested a crosslinking efficiency of 94 ± 5 % for H-1 and 82 ± 11 % for H-0.5. (Figure 1E)

LM was also optionally introduced in the hydrogel system as a surface coating, since this glycoprotein is abundantly found in endothelial cell BM.[18] The LM coating onto the hydrogel surface was confirmed by conjugating LM with a fluorophore (NHS-DyLight 488) (Figure 1F, Supporting Information).

2.2. Endothelial Cells' Tube Formation Assay Onto Hydrogels

ECs were seeded onto the hydrogels to evaluate tube formation in vitro under several different testing conditions (**Figure 2**A). Figure 2B,C illustrates ECs' ability to perform tube formation after 6 and 24 hours from seeding onto hydrogels with different crosslinking degree (H-1 and H-0.5), the addition of LM and VEGF (H-LM, H-LM-VEGF), and on Matrigel (Figure 2D). After 6 h (Figure 2B) on pristine hydrogels (H) ECs had a rounder shape, whereas on LM-coated samples (H-LM) and VEGF-supplied medium (H-LM-VEGF) they already appeared to be sprouting. Subtle but still notable differences can be appreciated between H-1 and H-0.5 hydrogels at this timepoint, with H-0.5 inducing more cellular organization. On the contrary, after 24 h (Figure 2C) differences in terms of ECs morphogenesis clearly emerged between H-1 and H-0.5 hydrogels. On H-0.5 hydrogels cells were indeed clustered in macroscopic tubule-like structures with a mean tube length of few hundred micrometers (300–400 µm) (Figure 2E) and a mean tube width of nearly 15 µm (Figure 2F), whereas on H-1 samples morphogenesis was a much more contained (tube length in the order of 100 µm and a tube width of 5 µm). As observed at the previous timepoint, on pristine hydrogels cells were still more circular in shape when compared to the H-LM and H-LM-VEGF counterparts (Figure 2G).

Nonetheless, on each condition, tubular structures proved to be stable for a longer time (>24 h) compared to commercially available materials (i.e., Matrigel) (Figure S4, Supporting Information) as demonstrated with live-dead staining (Figure 2H,I).

Finer details on ECs morphology could be assessed with DAPI and phalloidin fluorescent staining. From images (Figure 2L,M) it was evident that on H-0.5 samples cells had migrated toward each other to form big cell aggregates, a situation which is not induced on H-1 samples, where cells remained instead rounded and less organized. Despite that, with the addition of LM differences between H-1 and H-0.5 became less pronounced. As a matter of fact, adjacent cells were more elongated and protruding to form cell-cell interactions on both conditions, suggesting the importance of LM in sustaining ECs proliferation and network formation during angiogenesis through integrin binding.[39] Interestingly, conditions with medium supplemented with VEGF (100 ng mL^{-1}) gave different cellular responses depending on the hydrogels' crosslinking degree[19,26] Indeed, on H-1 samples ECs became flattened and proliferated all over the hydrogel surface, whereas on H-0.5 network branching was mildly improved.

Taken together, these results indicate that the ECs ability to perform tube formation was mainly determined by their interaction with the components of the hydrogel macromolecular backbone (i.e., gelatin and chondroitin sulfate) and not by the free VEGF added in the medium. These findings make the GEL-5MF:CS-5MF % w/w ratios, the crosslinking degree and the LM coating, the pivotal parameters to control for the rational design of hydrogels mimicking the BM.

2.3. Studies of Hydrogel Viscoelastic Behavior at the Macro and Microscale

Since the hydrogel crosslinking degree was a key factor in determining ECs phenotype during the tube formation assay, further experiments were performed to deeply investigate how hydrogels' mechanical properties could be modulated. Rheological characterization of H-1 and H-0.5 hydrogels was conducted using both macroscale (rheometer) and micro/nanoscale (AFM) approaches to comprehensively assess their viscoelastic behavior.

Measurements performed by AFM revealed the hydrogels' spatially localized mechanical properties as well as frequency-dependent viscoelastic behavior up to 500 Hz. For both hydrogel formulations (H-1 and H-0.5) and across both timepoints (0 and 24 h), AFM frequency sweeps (**Figure 3**A,B) confirmed a dominant elastic component (G′), although G″ progressively approached and surpassed G′ at high frequency. Specifically, the crossover point (i.e., where G″ exceeded G′) was observed at 220 Hz for H-0.5 and at 100 Hz for H-1, suggesting that both hydrogels made a transition toward a more viscous behavior.[40]

In Figure 3C,D are reported the Young's moduli evaluated from the approaching curve before the application of the corresponding frequency. Young's moduli were found to be rather consistent across the samples in the entire frequency range tested, both before and after swelling in the medium, attesting no aging effect upon mechanical perturbation. As expected, the Young's modulus of H-0.5 samples was found to be lower than H-1 due to lower crosslinking degree. This softening effect was also reflected in the hydrogel network morphology, as H-0.5 hydrogels had a much more porous structure than H-1 (Figure 3L,M).

AFM-based measurements further highlighted time-dependent softening of hydrogels in culture conditions. For H-1, G′ decreased from 2920 ± 990 Pa at 0 h to 320 ± 150 Pa after 24 h (Figure 3E), while Young's modulus (E) dropped from 3830 ± 310 to 510 ± 10 Pa (Figure 3F) over the same time period. Similarly, H-0.5 showed a reduction in G′ from 530 ± 240 to 37 ± 21 Pa and in E from 750 ± 53 to 81 ± 4 Pa. This marked reduction in mechanical parameters is likely due to progressive hydration and/or weight loss of the hydrogel network in cell culture medium during the 24 h of incubation (Figure 3G).[41,42]

Frequency sweeps (Figure 3H) performed with the rheometer confirmed that both hydrogels exhibit a predominant elastic response also in the macroscopic length scale over the tested

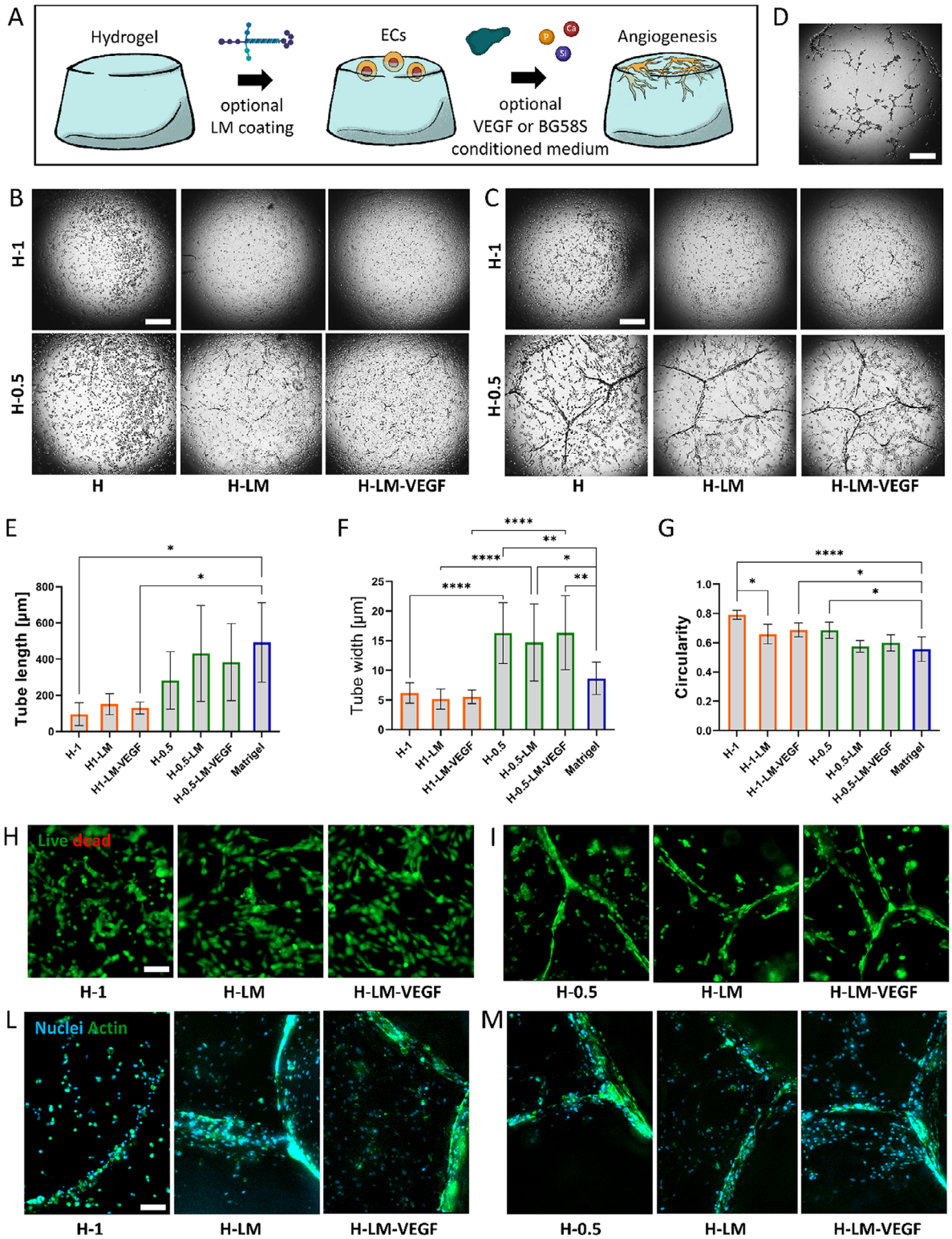

Figure 2. A) Illustration of tube formation assay on hydrogels. ECs tube formation assay after 6 h B) and 24 h C) from seeding onto H-1 and H-0.5 hydrogels. The pristine hydrogels (H) (left), with surface laminin coating (H-LM) (center), and with both surface laminin coating and medium supplemented with 100 ng of VEGF (H-LM-VEGF) (right). D) ECs tube formation assay after 6 h on Matrigel. ECs network analysis at 24 h: tube length E), tube width F), and cells' circularity G). A circularity value of 1.0 indicates a perfect circle. Live-dead staining of ECs tube formation assay after 24 h from seeding onto H-1 H) and H-0.5 I) for different conditions (H, H-LM, H-LM-VEGF). DAPI and Phalloidin-FITC staining of H-1 L) and H-0.5 M) hydrogels formulations at 24 h from seeding for different conditions (H, H-LM, H-LM-VEGF). Scale bar is 500 µm B,C,D), 200 µm H,I) and 100 µm L,M). Data ($n = 3$) are presented as mean ± SD. Non-significant (ns), $p > 0.05$, *$p \leq 0.05$, **$p \leq 0.01$, ****$p \leq 0.0001$.

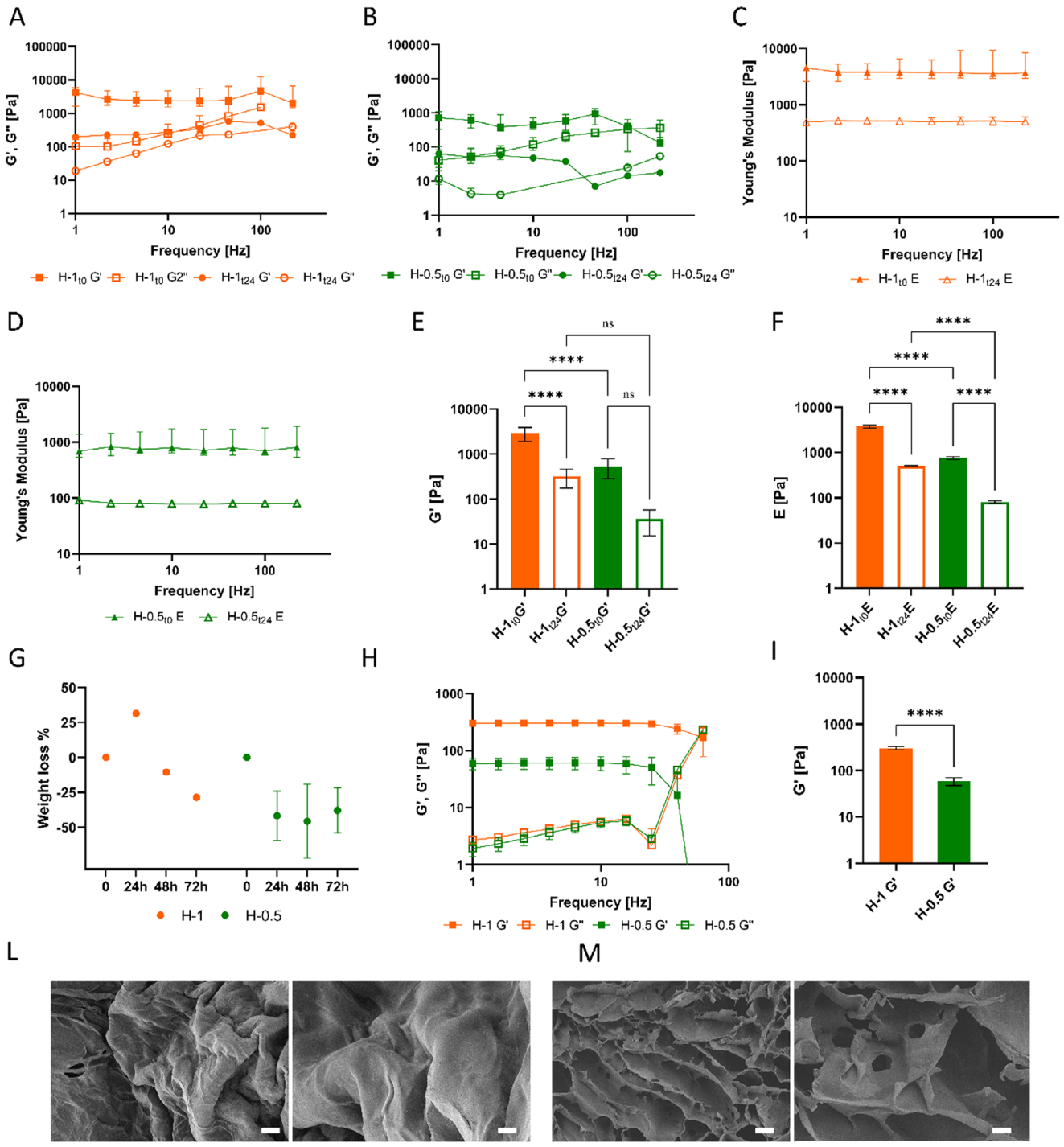

Figure 3. Frequency sweeps curves obtained with AFM of H-0.5 A) and H-1 B) hydrogels before and after 24 h of swelling in the medium. Young's modulus as a function of frequency calculated with AFM for H-1 C) and H-0.5 D), before and after swelling in the medium. G′ values E) and E values F) of both hydrogel formulations before (t0) and after (t24) swelling in the medium. G) Weight loss % of hydrogel formulations when imbibed in PBS (37 °C, 5% CO_2, humidity 100%). H) Frequency sweeps curve of H-0.5 and H-1 hydrogels obtained with the rheometer and associated G′ values I). SEM images of H-1 L) and H-0.5 M) samples at two different magnifications. Scale bar is 100 µm (left) and 20 µm (right). Data ($n = 3$) are presented as mean ± SD. Non-significant (ns), $p > 0.05$, **** $p \leq 0.0001$.

frequency range (<100 Hz), with a mean storage modulus (G′) value of 300 ± 3 Pa for H-1 and 58 ± 2 Pa for H-0.5 (Figure 3I).

Collectively, these findings support the notion that H-1 and H-0.5 hydrogels possess a predominantly elastic character, with a viscous dissipation becoming relevant only at high-frequency regimes, at both length scales. Nonetheless, AFM-derived G′ are substantially higher than those measured via rheometer. This discrepancy between AFM and rheometer-derived values of G′ is attributed to the different length scales at which the two techniques operate. Indeed, the micro/nanoscale probing of AFM may result in higher substrate stiffness values due to microstructural features or inhomogeneities not captured in bulk measurements across the entire sample.[43] It is worth highlighting that the cellular length scale is similar to that one at which AFM operates, making AFM-derived stiffness measures more relevant than those performed with traditional rheology.[44]

These results can explain the different behavior displayed by ECs on the hydrogel during angiogenesis, making it plausible that a substrate with an elastic modulus in the order of ≈80 Pa (H-0.5) can promote a more efficient tube formation due to enhanced cellular mobility.[26]

Since the H-0.5 hydrogel was superior in inducing ECs to form a pseudo-capillary network in vitro, it was used for further experiments.

2.4. Bioactive Glass 58S Characterization After Exposure to Endothelial Cells' Culture Medium

Bioactive glasses can act as an angiogenic promoter capable of boosting vascularization of 3D constructs through ions (e.g., Ca, Si) release.[30,32] Experiments were thus performed aiming at characterizing BG58S bioactivity after exposure to ECs culture medium. We decided to test bioactivity by exposing BG58S directly to cell culture medium instead of simulated body fluid (SBF), since the glass degradation process is tightly dependent on the solution composition. To this purpose, ECGM was conditioned with different concentrations (i.e., 0.5, 1, 2.5, 5, 10 mg mL^{-1}) of BG58S for 2 or 24 h. Afterwards, we studied both the formation of hydroxycarbonate apatite (HCA) on the glass surface and, most importantly, the ions' (i.e., Ca, Si, P) release profiles in the culture medium.

The surface of the unreacted BG58S has an intrinsic porous texture (**Figure 4A**). However, from SEM images it can be appreciated that already after 2 h from immersion in culture medium, the glass surface appeared completely covered by very small precipitates of crystalline HCA layer for both 1 and 5 mg mL^{-1} concentrations (Figure 4B,C).[45]

Surface changes attesting bioactivity were further confirmed by FT-IR spectra (Figure 4D,E). A characteristic band at 875 cm^{-1} started developing at 1 mg mL^{-1} and increased in intensity as glass concentration increased, which has been assigned to C—O stretching from CO_3^{-2} being incorporated into the calcium-phosphate film to form HCA. Also, the bending vibrations of phosphate groups (P—O) in the crystalline phase of the HCA were clearly found at 571 and 603 cm^{-1} for glass concentrations between 0.5 and 10 mg mL^{-1}.[46]

When placed in solution, ions were released from the glass network, with cations exchanging with H^+ ions from the medium. Deposition of HCA at the bioactive glass surface follows the cation exchange. Dissolution was confirmed by ICP analysis, which quantifies elemental concentration in solution, showing that both Ca and Si generally increased in the media as initial glass content increased (Figure 4F,G). Si release is expected to be in the form of SiO_4^{4-}. Ca concentration (Ca^{2+}) rose from a basal level of 58.8 ± 0.7 μg mL^{-1} to almost 200 μg mL^{-1} for the highest BG58S initial concentrations (5 and 10 mg mL^{-1}) and conditioning times (24 h); Si content in the media increased from 0.4 ± 0.1 μg mL^{-1} to a maximum of nearly 50 μg mL^{-1} (BG58S 10 mg mL^{-1}, 24 h). Consistently with the SEM observation, P displayed the opposite behavior since it precipitated from the solution to form the calcium-phosphate layer onto the glass surface (Figure 4H), dropping from 19.9 ± 0.5 to 0.4 ± 0.1 μg mL^{-1}.

The pH also showed a positive correlation with initial glass content due to increased cations (Ca^{2+}) exchange with protons (H^+/H_3O^+) present in solution (Figure S5, Supporting Information).

Despite the extended surface area of BG58S powder, which conferred a high reactivity to the glass when immersed in physiological solutions,[47] it was possible to attest that there were significant differences in terms of ion concentrations between media conditioned for 2 and 24 h for almost all conditions.

2.5. Effect of BG58S-Conditioned Medium on Endothelial Cells Angiogenesis

To explore the biological effects of Ca and Si released from the bioactive glass on ECs, culture medium was conditioned with BG58S powder and biochemical assays were performed.

Viability was first analyzed via AlamarBlue. Medium conditioned for 2 h with BG58S at 1, 2.5, and 5 mg mL^{-1} concentrations resulted in an ECs' viability increase (>1.5-fold change), whereas 10 mg mL^{-1} was found to decrease it (0.6-fold change) (**Figure 5A**). Interestingly, when the medium was conditioned with BG58S for longer time (24 h) (Figure 5B) all conditions resulted instead in a decreased viability (1 mg mL^{-1} = 0.9-fold change; 2.5 mg mL^{-1} = 0.9-fold change; 5 mg mL^{-1} = 0.4-fold change; 10 mg mL^{-1} = 0.1-fold change) except for the lowest BG58S concentration, where no variation in viability was observed (0.5 mg mL^{-1} = 1.0-fold change). The beneficial effect on ECs viability of 2 h conditioning with BG58S can be ascribed to Si and Ca ions released in the medium, which were reported to effectively promote the angiogenic behavior of ECs by increasing their proliferation.[28] Nonetheless, the reversed biological effect observed at 24 h reflected the release profiles recorded through ICP analysis, suggesting that the ion levels became toxic for ECs survival, which is common in in vitro studies.

Given the fact that culture medium conditioned with 1 to 5 mg mL^{-1} of BG58S powder for 2 h gave the best viability increment within the shortest window of time, 5 mg mL^{-1} was chosen as the glass concentration for further experiments.

Tube formation kinetics on H-0.5 hydrogels increased as ECs managed to complete mesh formation more rapidly in the presence of BG58S-conditioned medium (H-BG) than the control condition (H). As shown in Figure 5C,D, in H-BG samples capillary morphogenesis was completed after just 18 h from seeding, as at 24 h there was no further improvement in terms of mesh

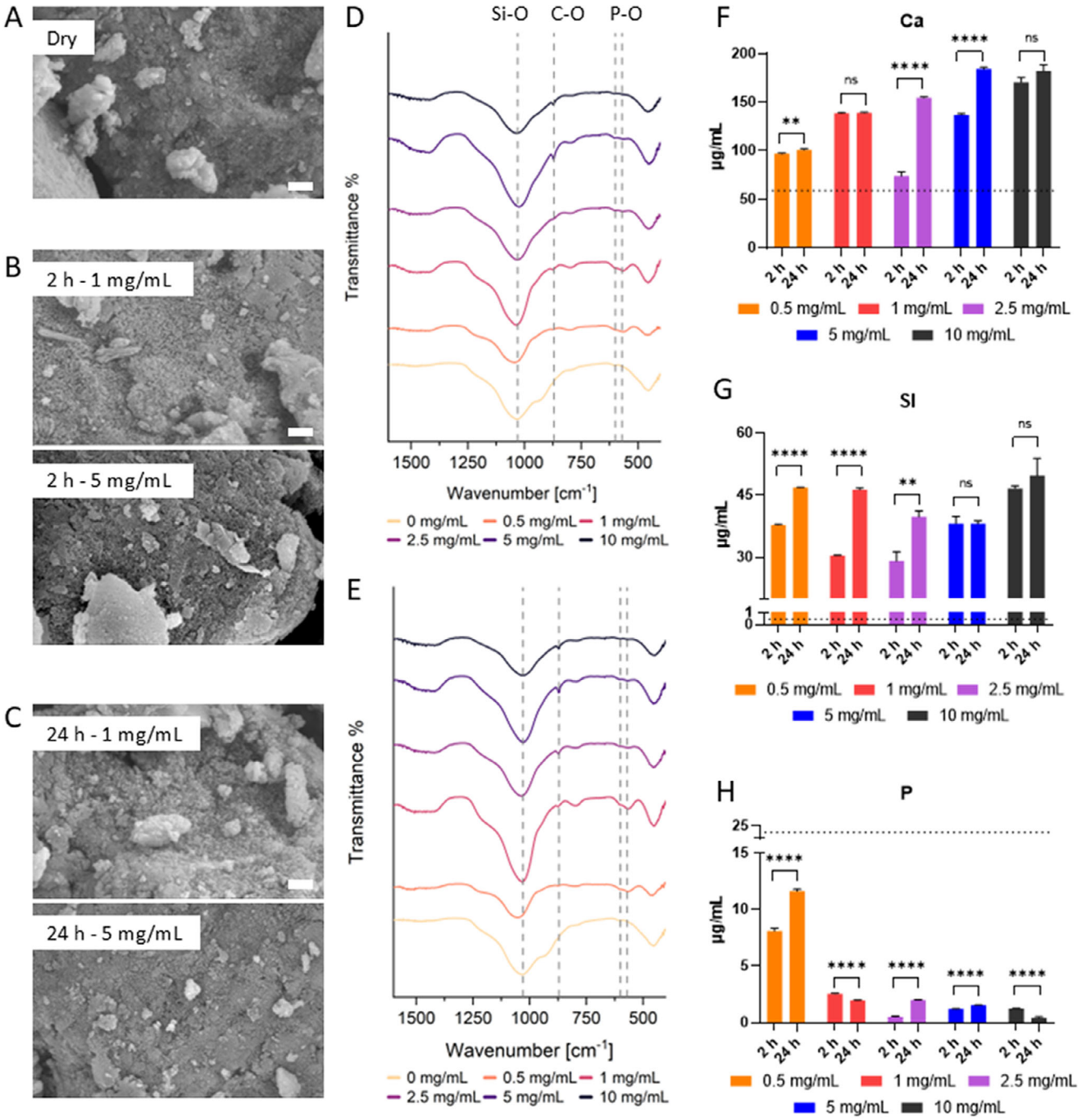

Figure 4. SEM images of dry BG58S A) and after exposure to cell culture medium for 2 h B) and 24 h C) at a concentration of 1 (top) and 5 mg mL^{-1} (bottom). Scale bar is 200 nm. FT-IR spectra of BG58S powder after exposure to cell culture medium for 2 D) and 24 E) h at different concentrations (0.5, 1, 2.5, 5, 10 mg mL^{-1}). Dashed lines indicate: P—O bend at 571 and 603 cm^{-1}, C—O stretch at 870 cm^{-1}, Si—O stretch at 1030 cm^{-1}. ICP analysis of cell culture medium conditioned with 0.5, 1, 2.5, 5, and 10 mg mL^{-1} of BG58S for 2 and 24 h for calcium F), silicon G) and phosphorus H). The dashed lines represent the basal ion concentrations in the ECGM. Data ($n = 3$) are presented as mean ± SD. Non-significant (ns), $p > 0.05$, ** $p \leq 0.01$, **** $p \leq 0.0001$.

organization, whereas on control samples (H) angiogenesis was completed only after 24 h.

We then hypothesized that this enhanced tube formation performance might again be attributable to Ca ions and Si species present in the conditioned medium via the preferential activation of genes involved in the process, especially those mediating cell adhesion, interaction, migration, and ECM remodeling.[34,48,49] Gene expression of platelet endothelial cell adhesion molecule (CD31), vascular endothelial cadherin (VE-Cadherin), vascular endothelial growth factor receptor 2 (VEGFR-2), and matrix

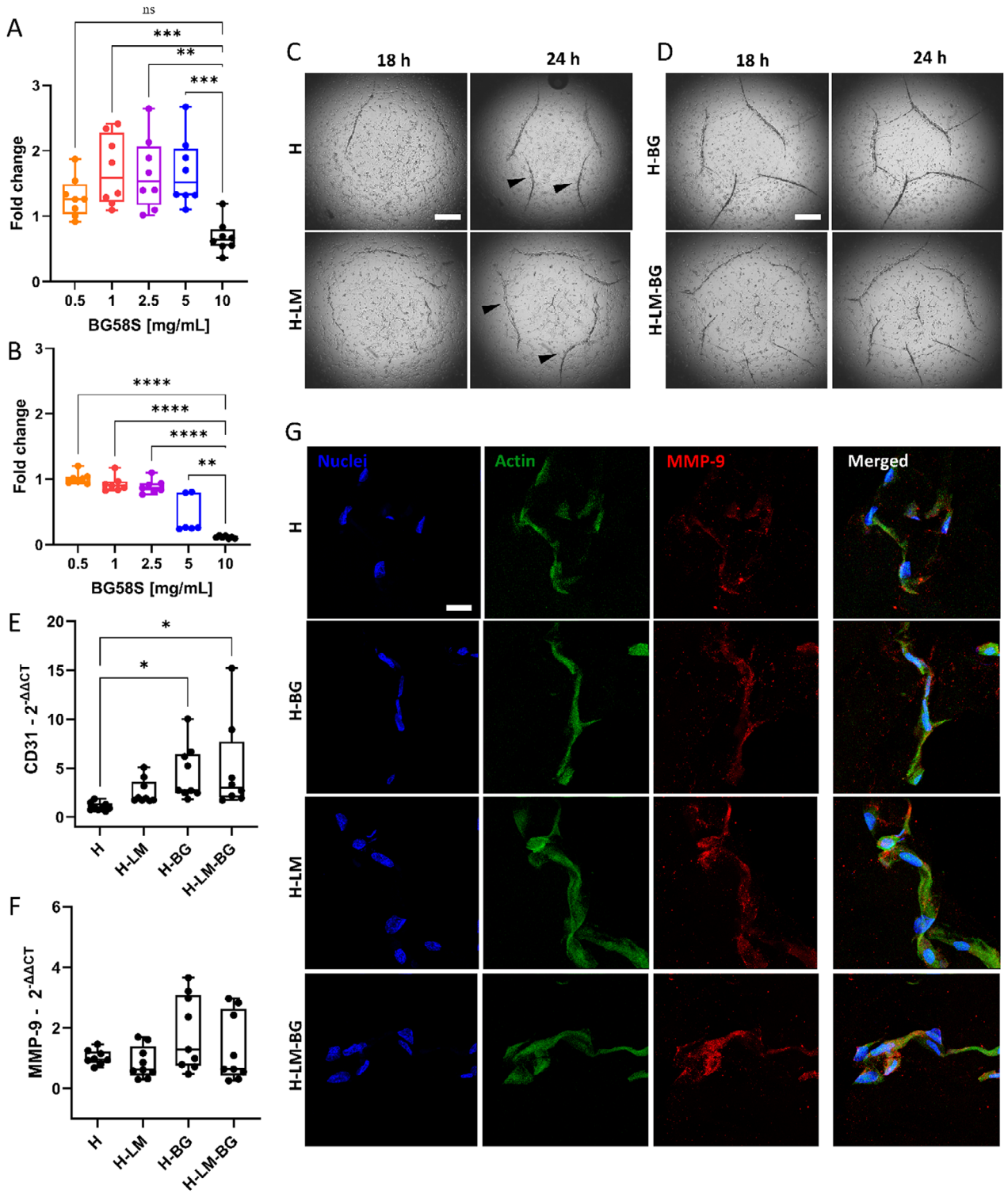

Figure 5. Effect on ECs viability with medium conditioned with increasing concentrations (from 0.5 to 10 mg mL^{-1}) of BG58S for 2 h A) and 24 h B). BG58S effect on ECs angiogenesis onto H-0.5 hydrogels. C) Phase contrast images of ECs tube formation assay on pristine hydrogel (H) (top) and with laminin coating (H-LM) (bottom) after 18 (left) and 24 (right) hours from seeding, and D) with the addition of culture medium conditioned for 2 h with 5 mg mL^{-1} of BG58S. Black arrows indicate new tubule morphogenesis. Gene expression analysis of CD31 E) and MMP-9 F) obtained through qPCR after 24 h from seeding. Data are presented as fold change relative to H calculated with the $2^{-\Delta\Delta CT}$ method. G) Immunofluorescence staining of MMP-9 at 24 h from seeding for H, H-BG, H-LM, and H-LM-BG samples. Counterstain with DAPI (nuclei) and phalloidin-FITC (actin). Scale bar is 500 µm in C and D and 20 µm in G. In the box plots the median is shown as a black line; boxes represent the 25th to 75th percentiles and whiskers extend from the minimum to the maximum values. Data (n = 3) are presented as individual values. Non-significant (ns), $p > 0.05$, * $p \leq 0.05$, ** $p \leq 0.01$, *** $p \leq 0.001$, **** $p \leq 0.0001$.

metalloproteinases 9 (MMP-9) was thus analyzed with qPCR (Figure 5E,F; Figure S6, Supporting Information).[50–52] Interestingly, CD31 turned out to be upregulated (5-fold change) in H-BG and H-LM-BG, as well as VE-Cadherin (2.5-fold change in H-BG). VEGFR-2 was also upregulated in H-LM-BG (2-fold change). Finally, MMP-9 expression levels had a nearly 2-fold increase in the H-BG conditions.

ECs production of MMP-9 could also be visualized through immunofluorescence. These enzymes are in fact engaged in matrix remodeling in order to ECs to sprout and generate new capillaries.[18] Figure 5G shows MMP-9 both on the cell membrane and in the nearby extracellular space, attesting that the molecular machinery for ECM degradation was active in all conditions. However, a burst in MMP-9 signal (red channel) (Figure S7, Supporting Information) was observed when ECs were cultivated in the presence of BG58S-conditioned medium and/or the LM coating, suggesting a further post-transcriptional control of MMP-9 expression.

Taken together, these results attested the ability of BG58S to boost tube formation morphogenesis by triggering multiple signal transduction pathways, in particular by promoting the expression of endothelial junction-associated molecules and the secretion of matrix remodeling enzymes. The use of inorganic agents in GAG-based instructive biomaterials for angiogenesis could therefore bypass some drawbacks related to growth factors delivery (e.g., short half-life and high concentration), leading to a faster approval from the FDA and therefore, a smoother clinical translation.[31]

3. Conclusion

In this study, we successfully developed and characterized a novel, growth factor-free hydrogel system composed of adhesive proteins (GEL and LM) and negatively charged GAGs (CS) capable of interacting with charged species (VEGF and cations), demonstrating its significant potential to promote in vitro angiogenesis.

By precisely tuning the material Young's Modulus by changing the hydrogel crosslinking degree, it was observed a marked enhancement in ECs attachment and migration ability on softer substrates (H-0.5) (γ = 50 %; E ≈80 Pa), which is a critical early step of the blood vessel formation mechanism. Furthermore, tube formation assay on H-0.5 formulation outperformed commercial ECM extracts (e.g., Matrigel) in terms of ECs tubes' size and stability over time.

Crucially, we demonstrated that the released species of BG58S, specifically of Ca and Si ions, could act as potent angiogenic promoters. Indeed, the incorporation of these inorganic ions into the culture medium not only improved ECs viability but also significantly accelerated the kinetics of tube formation onto hydrogels, achieving results comparable to those typically requiring exogenous growth factor supplementation (i.e., VEGF) above physiological concentrations.

Last, qPCR experiments attested an upregulation of genes encoding for endothelial-specific adhesion molecules (CD31 and VE-Cadherin), cell proliferation, survival and migration (VEGFR-2), and ECM remodeling (MMP-9), while immunofluorescence staining proved an increased localization of MMP-9 on both the ECs membrane and in the nearby extracellular space when culture medium was conditioned with BG58S and/or the hydrogel's surface was covered with LM.

The proposed strategy involving the dual use of sulfated GAG-based hydrogels and BG58S dissolution products to boost angiogenesis represents a substantial advancement in the field of tissue engineering. We believe that this innovative approach offers a highly promising and valuable strategy to overcome the persistent challenge of vascularizing 3D cellular constructs in vitro, paving the way for the successful clinical translation of engineered tissues and organs.

4. Experimental Section

Materials: CS (Mw 30000; Purity >90%; Biosynth), gelatin type A (GEL), 4arm-polyethileneglycole-maleimide (4arm-PEG10k-Maleimide) (Mn 10000), 5-methylfurfural, 5-methylfurfurylamine (TCI), sodium cyanoborohydride ($NaBH_3CN$), mouse LM, VEGF, BG58S powder (60 mol % SiO_2, 36 mol % CaO, 4 mol % P_2O_5; particle size ≤10 µm), Ca (19 051), P (38 338), Si (0 8729) standards for ICP. All reagents were purchased from Merck unless otherwise specified.

Materials Functionalization: GEL and CS were functionalized with 5-methylfurfural and 5-methylfurfurylamine, respectively as previously reported.[53–56] In brief, 100 eq (3.4 mL) of 5-methylfurfural were added to a solution of GEL (1 g in 15 mL of PBS pH 5.5). After 30 min 50 eq (1.2 g) of $NaBH_3CN$ were added, and the mixture was stirred at 40 °C for 24 h. Equivalents were calculated on the total amount of lysine (5–7 % w/w) present in the GEL. To a solution of CS (1 g in 15 mL of MES buffer pH 5.5), 1 eq of EDC and 1 eq of NHS (0.4 and 0.2 g) were added in this order. After 30 min 1.5 eq (0.3 mL) of 5-methylfurfurilammine were added drop by drop and stirred overnight at 40 °C. Equivalents were calculated on the total amount of COOH groups present in CS.

Solutions were dialyzed against a NaCl solution (0.1 M) for 1 day, followed by distilled water for 4 days, using 14 and 1 kDa dialysis membranes for functionalized GEL and CS, respectively. The dialyzed solutions were freeze-dried and kept under vacuum at −20 °C until usage.

The degree of functionalization (DoF) was calculated with ^{1}H NMR spectroscopy using the software MNova (Mestrelab research).

Hydrogels Crosslinking: GEL-5MF, CS-5MF, and 4arm-PEG10k-Maleimide were dissolved in PBS (pH 7.4) separately at a concentration of 100 mg mL^{-1} and were kept at the thermomixer (37 °C, 1200 rpm) until complete dissolution. Materials were then diluted and mixed to generate hydrogels with different GEL-5MF:CS-5MF % w/w ratios (i.e., 2.5:0.5, 2:1, 0.5:2.5) and crosslinking degrees (i.e., 100% and 50%). γ % was calculated considering the DoF of GEL-5MF and CS-5MF. Hydrogels were always kept overnight in incubator (37 °C, 5 % CO_2, 100 % humidity) to allow full crosslinking.

Rheological Analysis: A 2 mL of hydrogel formulations were crosslinked in Eppendorf. Rheological measurements were performed with a rheometer (MCR 92e, Anton Paar), using a parallel-plate geometry with a diameter of 50 mm and gap height of 1 mm. Frequency sweeps analysis (frequency from 0.1 to 100 Hz; shear strain = 1 %; T = 37 °C) were used to evaluate G′ and G″.

Hydrogels Physicochemical Characterization: GEL-5MF and CS-5MF were diluted to 20 and 10 mg mL^{-1}, respectively (GEL-5MF:CS-5MF w/w % ratio 2:1), whereas 4arm-PEG10k-Maleimide was diluted either to 22 or 11 mg mL^{-1} in order to obtain a crosslinking degree (γ of 100 (H-1) and 50 % (H-0.5).

H-1 and H-0.5 hydrogels were prepared in cylindrical molds (height = 10 mm; diameter = 5 mm).

Hydrogels were lyophilized for analysis at scanning electron microscopy (SEM) and Fourier transform infrared (FT-IR) spectroscopy. SEM images were taken at 5 kV and prior graphite sputtering (ZEISS Gemini 500 field emission HR-SEM). FT-IR spectra were recorded in attenuated total reflection (ATR) mode from 4000 to 550 cm^{-1} (4 cm^{-1} resolution, 32 scans) (PerkinElmer Spectrum 100).

Hydrogels employed for calculating weight loss (W %) measurements were imbibed in PBS (pH 7.4) in cell culture conditions (37 °C, 5 % CO_2, 100 % humidity). W % was calculated as follows:

$$W\,\% = \frac{Wf - Wi}{Wi} \cdot 100 \quad (1)$$

where W_f is the weight of the hydrogel at desired timepoint and W_i is the weight of the hydrogel post synthesis.

Hydrogels employed for calculating gel fraction % were dried in the oven at 40 °C for 4 h and then imbibed in PBS (pH 7.4) in cell culture conditions overnight. Gel fraction % was calculated as follows:

$$\text{Gel fraction}\,\% = \frac{Ws}{Wd} \cdot 100 \quad (2)$$

where *Ws* is the weight of the dried hydrogel after swelling and *Wd* is the weight of the dried hydrogel post-synthesis.

Cell Culture: Human umbilical vein endothelial cells (HUVEC) (PromoCell) were cultivated in endothelial cell growth medium (ECGM) (PromoCell) supplemented with Supplementpack aliquots (PromoCell). Penicillin-streptomycin (1 % v/v) (Euroclone) and Amphotericin B (1 % v/v) (Euroclone) were also added to the medium. Cells were maintained at 80–90% confluency. HUVEC were used between passage 5 and 8 for all experiments as recommended.[14]

Tube Formation Assay on Hydrogels: Materials were weighed and sterilized for 30 minutes under UV light. Then, 50 µL of H-1 and H-0.5 hydrogels were prepared into 96-well plates and were then left in incubator overnight.

Different conditions were tested, namely: H-1, H-0.5, hydrogels coated with LM (H-LM), and with the addition in the medium of 100 ng mL^{-1} of VEGF (H-LM-VEGF).

H-LM hydrogels were coated with 50 µL of a LM solution to reach a final coverage of 5 µg cm^{-2}. After 1.5 h, LM solution was removed. LM coating was confirmed by labelling LM with a fluorescent NHS tag (DyLight 488 NHS Ester, Thermo Fisher Scientific).

HUVEC were seeded onto hydrogels (45000 cells cm^{-2}) in a total volume of 100 µL. After 2 h from seeding, another 100 µL of medium was added to the culture.

Images were taken at different timepoints (6 h and 24 h from seeding) by phase contrast and fluorescence microscopy. For fluorescence microscopy, cells were either stained directly in the culture for 30 min with 100 µL of live-dead solution (Calcein-AM 2 µM; Propidium iodide 4 µM) (Thermo Fisher Scientific) or fixed with a paraformaldehyde solution (4 % v/v), permeabilized with Triton X-100 (0.1 % v/v), and stained with 25 µL of DAPI and 25 µL of phalloidin-FITC solutions. Phase contrast images were used to quantify tube length, tube width and cell circularity with the software ImageJ. Region of interest (ROI) of 322 x 322 µm were used.

AFM Measurements: H-1 and H-0.5 hydrogels were prepared in cylindrical molds (height = 3 mm; diameter = 3 mm). After demolding, samples were transferred into petri dishes for AFM analysis. Measurements were performed in liquid (ECGM) using an atomic force microscope (Nanowizard 4XP, Bruker) equipped with a pyramidal square-based tip (MLCT-BIO Tip E, Bruker Probes). The AFM tip was brought into contact with the hydrogel surface and indented until a force setpoint of 0.75 nN was reached. The tip position was then held constant for 8 s to allow for stress relaxation, followed by a frequency sweep in a logarithmic scale from 1 to 500 Hz. Each frequency point consisted of 20 sinusoidal cycles with an amplitude of 50 nm. Force data were used to estimate the storage (G′) and the loss (G″) moduli. Additionally, the Young's modulus was extrapolated by fitting the force–distance approach curves with the Hertz–Sneddon model.[57] Analysis was performed in at time 0 and after 24 h of swelling in cell culture medium.

BG58S Characterization After Exposure to Cell Culture Medium: BG58S was added to ECGM to reach the final concentrations of 0.5, 1, 2.5, 5, and 10 mg mL^{-1} and was left shaking at RT. pH was monitored within the first 24 h using a bench pH meter.

At desired timepoints (2 h and 24 h), conditioned medium was centrifuged, filtered (0.45 µm) and diluted by a factor of 10 with 2 M HNO_3 for analysis at inductively coupled plasma-optical emission spectrometry (ICP-OES) (iCAP 6300 Duo, Thermo Scientific). Mixed standards of Ca, Si and P (0, 0.1, 0.2, 0.4, 0.8, 1, 5, 10, and 20 µg mL^{-1}) were prepared in 2 M HNO_3 for the calibration curve and ECGM was used as reference. P was measured in the axial direction of the plasma flame, whereas Ca and Si were measured in the radial direction.

BG58S exposed to culture medium was instead washed with MilliQ water for 1 h on a shaking plate. Then, it was centrifuged to eliminate unbound impurities and dried at 60 °C in the oven for 4 hours before SEM and FT-IR spectroscopy.

For SEM analysis, BG58S powder was previously fixed with conductive adhesive on aluminum supports and coated with graphite. Images were then taken at 5 kV. FT-IR spectra were recorded in attenuated total reflection (ATR) mode from 1600 to 400 cm^{-1} (2 cm^{-1} resolution, 32 scans).

Cell Viability Assessment: Culture medium was conditioned by adding BG58S at different concentrations (1, 2, 5, 10, and 20 mg mL^{-1}) for 2 or 24 h. Medium was then centrifuged (1000 rpm; 5 min) and filtered (0.22 µm). HUVEC were seeded in 96-well plates at a seeding density of 5000 cells/cm^2 in 100 µL of medium. After 4 hours from seeding 100 µL of BG58S-conditioned medium was added to each condition to the following final dilution (0.5, 1, 2.5, 5, and 10 mg mL^{-1}).

After 24 h viability was assessed using AlamarBlue (Invitrogen). To this purpose, medium was removed from wells and AlamarBlue was diluted in fresh medium (1:10) and 200 µL were added to the culture. Cells were left in the incubator for 2 h. Afterwards, 100 µL of medium were transferred to empty wells and absorbance was read at 570 and 600 nm.

Resazurin reduction percentage (r %) was calculated as reported in the datasheet using as negative control the cell culture medium with the diluted (1:10) AlamarBlue reagent but without cells. Viability was reported as a fold change of r % compared to the positive control (HUVEC cultured in medium without BG58S).

BG58S Effects on Angiogenesis: ECGM medium was conditioned with BG58S (10 mg mL^{-1}) for 2 h. Tube formation was performed on H-0.5 samples, with and without LM coating. After 2 h from seeding 100 µL of BG58S-conditioned medium were optionally added to the culture (H-BG and H-LM-BG) to reach a final concentration of 5 mg mL^{-1}. Tube formation was evaluated at 18 and 24 h with phase contrast microscopy, and at 24 h with immunofluorescence and quantitative gene expression analysis.

Immunofluorescence Staining: Cells were fixed with a paraformaldehyde solution (4 % v/v), included in OCT and frozen at -20 °C for cutting at the cryostat. Slices were permeabilized with Triton X-100 (0.1 % v/v), and a bovine serum albumin (BSA) solution (3% w/v) was used for blocking. An anti-MMP-9 primary antibody (SAB5300247, Sigma-Aldrich) (final dilution 0.001 mg mL^{-1}) was left for 2 h at room temperature (RT) and after a secondary antibody (Anti-Mouse CF 568, Sigma-Aldrich) (1:1000 dilution) for 1 h at RT. 100 µL of a 1:1 solution made of DAPI and phalloidin-FITC was used as a counterstain. Finally, a water-soluble mounting medium (Fluoromount-G Mounting Medium) was used to mount stained hydrogels on glass slides.

MMP-9 area coverage % was calculated with the software ImageJ.

Real-Time Polymerase Chain Reaction (qPCR): Hydrogels were minced and transferred in Eppendorf. 1 mL of TRIzol (Invitrogen) was added and samples were stored at −80 °C. After three steps of freeze-thawing, samples were centrifuged (12000 rpm; 5 min; 4 °C) to remove hydrogel fragments. The supernatant was transferred into new Eppendorf, mixed with 200 mL of chloroform, and centrifuged (12000 rpm; 15 min; 4 °C). The aqueous phase was then collected, mixed with 500 mL of isopropanol and left at −20 °C. The day after, samples were centrifuged (12000 rpm; 15 min; 4 °C), the supernatant was discarded, and the precipitated RNA was resuspended in RNase-free water. The RNA concentration and the 260/280 and 260/230 values were measured using a microvolume spectrophotometer (NanoDrop, Thermo Fisher Scientific).

cDNA was synthesized from 200 ng of RNA, using iScript cDNA Synthesis Kit (Bio-Rad), following the manufacturer's protocol. The obtained cDNA was diluted in RNase-free water to a concentration of 2 ng μL^{-1}.

10 µL composed of 2 µL of cDNA (4 ng), 5 µL of Luna Universal qPCR Master Mix (New England Biolabs), and 3 µL of reverse and forward primer

mix (1.25 µM) (Table S2, Supporting Information) were prepared in 96-well reaction plate of 0.1 mL (Applied Biosystems). Finally, qPCR was conducted using a 7900HT system (Thermo Fisher Scientific) with a thermal cycle of 95 °C for 15 s, 55 °C for 15 s, and 60 °C for 30 s. The $2^{-\Delta\Delta Ct}$ method was employed to calculate the relative gene expression, using B2M as the housekeeping gene and H samples as the control group for normalization.

Statistical Analysis: Data were always presented as mean ± standard deviation. Values were averaged from at least three repeated measurements (n = 3). To determine statistical difference between two groups unpaired two-tailed *t*-test was used, whilst comparing three or more groups was done with one-way ANOVA using Tukey's multiple-comparison test. Statistical significance of the data was calculated at 95% ($P < 0.05$) confidence intervals. Non-significant (ns), $p > 0.05$, * $p \leq 0.05$, ** $p \leq 0.01$, *** $p \leq 0.001$, **** $p \leq 0.0001$.

Supporting Information

Supporting Information is available from the Wiley Online Library or from the author.

Acknowledgements

The authors thank Sara Curatolo for assistance with the preparation of the illustrations in Figures 1A and 2A. Ministero dell'Università e della Ricerca (MUR) PNC0000003 CUP BICOCCA B53C22006670001. Ministero della Salute RF-2021-12371959. Ministero dell'Università e della Ricerca (MUR) 2022MY7AZT. Fondazione Cariplo 2024-NAZ-0094 CUP BICOCCA H45E24000440007. Ministero dell'Università e della Ricerca (MUR) 2023-2027 - l. 232/2016, art. 1, commi 314–337. National Institute for Health and Care Research (NIHR) NIHR133314.

Conflict of Interest

The authors declare no conflict of interest.

Data Availability Statement

The data that support the findings of this study are openly available in Zenodo at [https://doi.org/10.5281/zenodo.17777638], reference number 17777637.

Keywords

angiogenesis, bioactive glass, ECM mimics, hydrogel, sulfated glycosaminoglycans, tissue engineering

Received: August 1, 2025
Revised: December 1, 2025
Published online: December 12, 2025

[1] T. Hoffman, A. Khademhosseini, R. Langer, *Tissue Eng., Part A* **2019**, *25*, 679.
[2] M. J. Webber, O. F. Khan, S. A. Sydlik, B. C. Tang, R. Langer, *Ann. Biomed. Eng.* **2015**, *43*, 641.
[3] D. Gholobova, L. Terrie, M. Gerard, H. Declercq, L. Thorrez, *Biomaterials* **2020**, *235*, 119708.
[4] D. S. Sparks, S. Saifzadeh, F. M. Savi, C. E. Dlaska, A. Berner, J. Henkel, J. C. Reichert, M. Wullschleger, J. Ren, A. Cipitria, J. A. McGovern, R. Steck, M. Wagels, M. A. Woodruff, M. A. Schuetz, D. W. Hutmacher, *Nat. Protoc.* **2020**, *15*, 877.
[5] S. Dalfino, E. Olaret, M. Piazzoni, P. Savadori, I. Stancu, G. Tartaglia, C. Dolci, L. Moroni, *Tissue Eng., Part A* **2025**, *31*, 13.
[6] B. O. Palsson, S. N. Bhatia, *Tissue Eng.* **2004**, 208.
[7] T. L. Place, F. E. Domann, A. J. Case, *Free Radical Biol. Med.* **2017**, *113*, 311.
[8] F. Iberite, M. Piazzoni, D. Guarnera, F. Iacoponi, S. Locarno, L. Vannozzi, G. Bolchi, F. Boselli, I. Gerges, C. Lenardi, L. Ricotti, *ACS Appl. Bio Mater.* **2023**, *6*, 2712.
[9] S. P. Herbert, D. Y. R. Stainier, *Nat. Rev. Mol. Cell Biol.* **2011**, *12*, 551.
[10] F. Cadamuro, F. Nicotra, L. Russo, *J. Controlled Release* **2023**, *354*, 726.
[11] J. Nicolas, S. Magli, L. Rabbachin, S. Sampaolesi, F. Nicotra, L. Russo, *Biomacromolecules* **2020**, *21*, 1968.
[12] F. Iberite, I. Gerges, L. Vannozzi, A. Marino, M. Piazzoni, T. Santaniello, C. Lenardi, L. Ricotti, *Ann. Biomed. Eng.* **2020**, *48*, 734.
[13] P. S. Briquez, L. E. Clegg, M. M. Martino, F. Mac Gabhann, J. A. Hubbell, *Nat. Rev. Mater.* **2016**, *1*, 15006.
[14] I. Arnaoutova, H. K. Kleinman, *Nat. Protoc.* **2010**, *5*, 628.
[15] S. Yang, J. Graham, J. W. Kahn, E. A. Schwartz, M. E. Gerritsen, *Am. J. Pathol.* **1999**, *155*, 887.
[16] P. Lu, D. Ruan, M. Huang, M.i Tian, K. Zhu, Z. Gan, Z. Xiao, *Signal Transduction Targeted Ther.* **2024**, *9*, 166.
[17] F. Cadamuro, M. Piazzoni, E. Gamba, B. Sonzogni, F. Previdi, F. Nicotra, A. Ferramosca, L. Russo, *Biomater. Adv.* **2025**, *175*, 214323.
[18] R. Kalluri, *Nat. Rev. Cancer* **2003**, *3*, 422.
[19] M. V. Tsurkan, K. Chwalek, S. Prokoph, A. Zieris, K. R. Levental, U. Freudenberg, C. Werner, *Adv. Mater.* **2013**, *25*, 2606.
[20] K. Chwalek, M. V. Tsurkan, U. Freudenberg, C. Werner, *Sci. Rep.* **2014**, *4*, 4.
[21] Y. D. P. Limasale, M. Fusenig, M. Samulowitz, P. Atallah, J. Sievers, N. Dennison, U. Freudenberg, J. Friedrichs, C. Werner, *Adv. Funct. Mater.* **2024**, *34*, 2411475.
[22] Y. D. P. Limasale, P. Atallah, C. Werner, U. Freudenberg, R. Zimmermann, *Adv. Funct. Mater.* **2020**, *30*, 2000068.
[23] S. Kühn, V. Magno, R. Zimmermann, Y. D. P. Limasale, P. Atallah, A. Stoppa, M. J. Männel, J. Thiele, J. Friedrichs, U. Freudenberg, C. Werner, *Adv. Mater.* **2025**, *37*, 2409731.
[24] E. Quinlan, S. Partap, M. M. Azevedo, G. Jell, M. M. Stevens, F. J. O'Brien, *Biomaterials* **2015**, *52*, 358.
[25] S. L. Jan, M. Hayashi, Z. Kasza, I. Eriksson, J. R. Bishop, I. Weibrecht, J. Heldin, K. Holmborn, L. Jakobsson, O. Söderberg, D. Spillmann, J. D. Esko, L. Claesson-Welsh, L. Kjellén, J. Kreuger, *Arterioscler., Thromb., Vasc. Biol.* **2012**, *32*, 1255.
[26] U. Freudenberg, J.-U. Sommer, K. R. Levental, P. B. Welzel, A. Zieris, K. Chwalek, K. Schneider, S. Prokoph, M. Prewitz, R. Dockhorn, C. Werner, *Adv. Funct. Mater.* **2012**, *22*, 1391.
[27] C. Kut, F. Mac Gabhann, A. S. Popel, *Br. J. Cancer* **2007**, *97*, 978.
[28] M. Šalandová, I. A. J. van Hengel, I. Apachitei, A. A. Zadpoor, B. C. J. van der Eerden, L. E. Fratila-Apachitei, *Adv. Healthcare Mater.* **2021**, *10*, 2002254.
[29] L. L. Hench, *J. Mater. Sci.: Mater. Med.* **2006**, *17*, 967.
[30] J. R. Jones, *Acta Biomater.* **2013**, *9*, 4457.
[31] S. Dalfino, P. Savadori, M. Piazzoni, S. T. Connelly, A. B. Giannì, M. Del Fabbro, G. M. Tartaglia, L. Moroni, *Adv. Healthcare Mater.* **2023**, *12*, 2300128.
[32] A. A. Gorustovich, J. A. Roether, A. R. Boccaccini, *Tissue Eng., Part B, Rev.* **2010**, *16*, 199.
[33] J. H. Lee, P. Parthiban, G. Z. Jin, J. C. Knowles, H. W. Kim, *Prog. Mater. Sci.* **2021**, *117*, 100732.
[34] C. Mao, X. Chen, G. Miao, C. Lin, *Biomed. Mater. (Bristol)* **2015**, *10*, 025005.
[35] P. Kastana, E. Choleva, E. Poimenidi, N. Karamanos, K. Sugahara, E. Papadimitriou, *FEBS J.* **2019**, *286*, 2921.
[36] D. Li, C. C. Clark, J. C. Myers, *J. Biol. Chem.* **2000**, *275*, 22339.

[37] F. Orozco, J. Li, U. Ezekiel, Z. Niyazov, L. Floyd, G. M. R. Lima, J. G. M. Winkelman, I. Moreno-Villoslada, F. Picchioni, R. K. Bose, *Eur. Polym. J.* **2020**, *135*, 109882.
[38] C. Nakason, K. Sasdipan, A. Kaesaman, *Iran. Polym. Journal (English Edition)* **2014**, *23*, 1.
[39] I. Arnaoutova, J. George, H. K. Kleinman, G. Benton, *Angiogenesis* **2009**, *12*, 267.
[40] J. Alcaraz, L. Buscemi, M. Grabulosa, X. Trepat, B. Fabry, R. Farré, D. Navajas, *Biophys. J.* **2003**, *84*, 2071.
[41] Y. Lai, Y. Hu, *Soft Matter* **2018**, *14*, 2619.
[42] R. Subramani, A. Izquierdo-Alvarez, P. Bhattacharya, M. Meerts, P. Moldenaers, H. Ramon, H. Van Oosterwyck, *Front. Mater.* **2020**, *7*, 212.
[43] C. F. Guimarães, L. Gasperini, A. P. Marques, R. L. Reis, *Nat. Rev. Mater.* **2020**, *5*, 351.
[44] M. D. A. Norman, S. A. Ferreira, G. M. Jowett, L. Bozec, E. Gentleman, *Nat. Protoc.* **2021**, *16*, 2418.
[45] P. Sepulveda, J. R. Jones, L. L. Hench, *J. Biomed. Mater. Res.* **2002**, *61*, 301.
[46] J. R. Jones, P. Sepulveda, L. L. Hench, *J. Biomed. Mater. Res.* **2001**, *58*, 720.
[47] D. M. M. dos Santos, G. L. de Oliveira, D. C. F. Soares, M. V. Maia, F. Tallia, A. Heyraud, J. Jones, M. Houmard, E. H. M. Nunes, *Mater. Chem. Phys.* **2025**, *332*, 130308.
[48] F. Monte, T. Cebe, D. Ripperger, F. Ighani, H. V. Kojouharov, B. M. Chen, H. K. W. Kim, P. B. Aswath, V. G. Varanasi, *J. Tissue Eng. Regener. Med.* **2018**, *12*, 2203.
[49] Y. Zhu, X. Zhang, G. Chang, S. Deng, H. F. Chan, *Adv. Mater.* **2025**, *37*, 2312964.
[50] H. M. DeLisser, M. Christofidou-Solomidou, R. M. Strieter, M. D. Burdick, C. S. Robinson, R. S. Wexler, J. S. Kerr, C. Garlanda, J. R. Merwin, J. A. Madri, S. M. Albelda, *Am. J. Pathol.* **1997**, *151*, 671.
[51] C. Lee, M. J. Kim, A. Kumar, H. W. Lee, Y. Yang, Y. Kim, *Signal Transduction Targeted Ther.* **2025**, *10*, 170.
[52] T. L. Haas, J. A. Madri, *Trends Cardiovasc. Med.* **1999**, *9*, 70.
[53] S. Magli, G. B. Rossi, G. Risi, S. Bertini, C. Cosentino, L. Crippa, E. Ballarini, G. Cavaletti, L. Piazza, E. Masseroni, F. Nicotra, L. Russo, *Front. Chem.* **2020**, *8*, 524.
[54] L. Rossi, C. Pignatelli, K. Kerekes, F. Cadamuro, A. Dinnyés, F. Lindheimer, J. Seissler, M. Lindner, S. Ziegler, P. Bartenstein, Y. Qiu, J. Kovács-Kocsi, Z. Körhegyi, M. Bodnár, E. Fazekas, E. Prépost, F. Nicotra, L. Russo, *Carbohydr. Polym. Technol. Appl.* **2024**, *8*, 100610.
[55] F. Cadamuro, L. Russo, F. Nicotra, *Eur. J. Org. Chem.* **2021**, *2021*, 374.
[56] S. Magli, L. Rossi, C. Consentino, S. Bertini, F. Nicotra, L. Russo, *Biomolecules* **2021**, *11*, 683.
[57] M. Sampietro, V. Cassina, D. Salerno, F. Barbaglio, E. Buglione, C. A. Marrano, R. Campanile, L. Scarfò, D. Biedenweg, B. Fregin, M. Zamai, A. Díaz Torres, V. Labrador Cantarero, P. Ghia, O. Otto, F. Mantegazza, V. R. Caiolfa, C. Scielzo, *HemaSphere* **2023**, *7*, 931.